

# Directed Lifting of Inversion Symmetry in Ruddlesden-Popper Oxide-Fluorides – Towards Ferroelectric and Multiferroic Behavior.

Ronghuan Zhang, Mark S. Senn and Michael A. Hayward\*.

Department of Chemistry, University of Oxford, Inorganic Chemistry Laboratory, South Parks Road, Oxford, OX1 3QR, United Kingdom.

**ABSTRACT:** The cooperative tilting distortions of  $n = 2$  Ruddlesden-Popper oxides can be utilized to break the inversion symmetry of the host lattice and induce ferroelectric behavior. Unfortunately the desired  $a^-c^+/a^-c^+$  structural deformation is only stabilized in phases with extremely small structural tolerance factors, limiting the chemical scope of this symmetry breaking approach. Here we describe the influence of topochemical fluorination on the structural distortions of  $n = 2$  Ruddlesden-Popper oxides and demonstrate that the conversion of  $\text{La}_3\text{Ni}_2\text{O}_7$  to  $\text{La}_3\text{Ni}_2\text{O}_{5.5}\text{F}_{3.5}$  breaks the inversion symmetry of the perovskite double-layers which constitute the Ruddlesden-Popper framework, by driving a change from an  $a^-c^0/a^-c^0$  distortion in the parent phase to an  $a^-c^+/a^-c^+$  distortion in the oxide-fluoride. In this instance, the symmetry breaking distortions of adjacent acentric perovskite sheets are anti-aligned, and as a result the inversion symmetry of the host lattice is broken locally, but not globally, resulting in an anti-ferroelectric structure. The breaking of local inversion symmetry in layered perovskite phases, in the absence of second-order Jahn-Teller active ‘distortion centers’, is an important step towards the realization of ferroelectric and multiferroic behavior in phases of this structure type.

## Introduction.

Magnetoelectric multiferroic materials – those which exhibit a combination of ferromagnetism and ferroelectricity – are highly desired due to the large number of applications such materials have. Unfortunately the preparation of phases which exhibit magnetoelectric behavior is extremely challenging.

The challenges associated with preparing magnetoelectric materials can be summarized simplistically by observing that while there are many known reliable methods of inducing and controlling ferromagnetism in materials,<sup>1-3</sup> the same cannot be said for ferroelectricity.<sup>4</sup> This difference arises from the different composition-structure-property relations of the two behaviors. Ferromagnetism requires a material to have ‘unpaired’ electrons, whose magnetic moments are coupled together to yield a collective spontaneous magnetization – a situation which can be achieved in a multitude of ways. In contrast, for a phase to exhibit ferroelectric behavior it must adopt a non-centrosymmetric (NCS) crystal structure<sup>5</sup> – this is a very specific and taxing requirement because in general centrosymmetric packing schemes are more efficient than asymmetric arrangements, and as a result NCS structures tend to be energetically disfavored with respect to centrosymmetric alternatives. These observations lead to the conclusion that the main challenge, when it comes to preparing novel magnetoelectric materials (or at least Type I magnetoelectric materials, where the microscopic origins of the ferromagnetism and ferroelectricity are independent), is inducing ferroelectric behavior rather than ferromagnetism.

The challenge presented by the preparation of ferroelectric

materials is one of long standing, and as a result a number of different strategies have been developed to try to overcome the inherent favorability of centrosymmetric structures, and prepare NCS phases. The most commonly adopted approaches utilize second-order Jahn-Teller (SOJT) distortions associated with either octahedrally coordinated  $d^0$  transition metal cations ( $\text{Ti}^{4+}$ ,  $\text{Nb}^{5+}$ ,  $\text{W}^{6+}$ , etc.),<sup>6-10</sup> or post-transition metal cations with  $ns^2$  electronic configurations ( $\text{Pb}^{2+}$ ,  $\text{Bi}^{3+}$ ),<sup>11-16</sup> to break the structural inversion symmetry of a phase, as observed for materials such as  $\text{BaTiO}_3$  and  $\text{BiFeO}_3$ . However the need to use symmetry-breaking SOJT cations in magnetoelectric materials is undesirable as it is both chemically limiting, and not immediately compatible with magnetism.<sup>17</sup> Given these issues, there has been a big effort to find further novel methods for inducing materials to adopt NCS crystal structures in the absence of SOJT cations.

Recently much attention has been focused on attempts to use the complex structural distortions observed in perovskite frameworks to prepare NCS phases.<sup>18</sup> This is an attractive approach because the  $\text{ABO}_3$  oxide perovskite structure can accommodate a very wide variety of different cations, including paramagnetic transition metal cations, and so doesn’t suffer from the restrictions inherent in the SOJT based approaches. Indeed, the desirable chemical flexibility of the perovskite structure can be attributed to these aforementioned structural distortions which occur via the cooperative twisting and tilting of the apex-linked  $\text{BO}_6$  octahedra which make up the perovskite network.

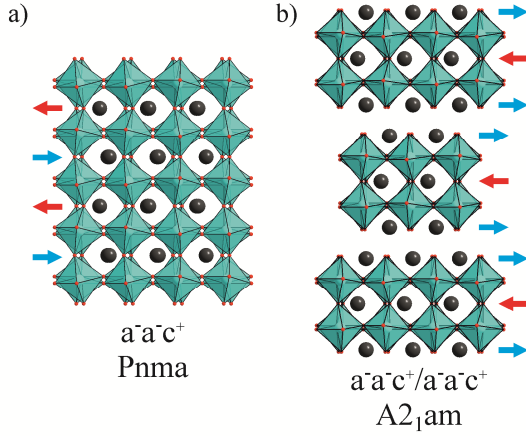


**Figure 1.** a) The ‘GdFeO<sub>3</sub> distorted’ perovskite structure and b) the  $n = 2$  Ruddlesden-Popper structure with an analogous structural distortion, which breaks the inversion symmetry of the lattice in the latter case.

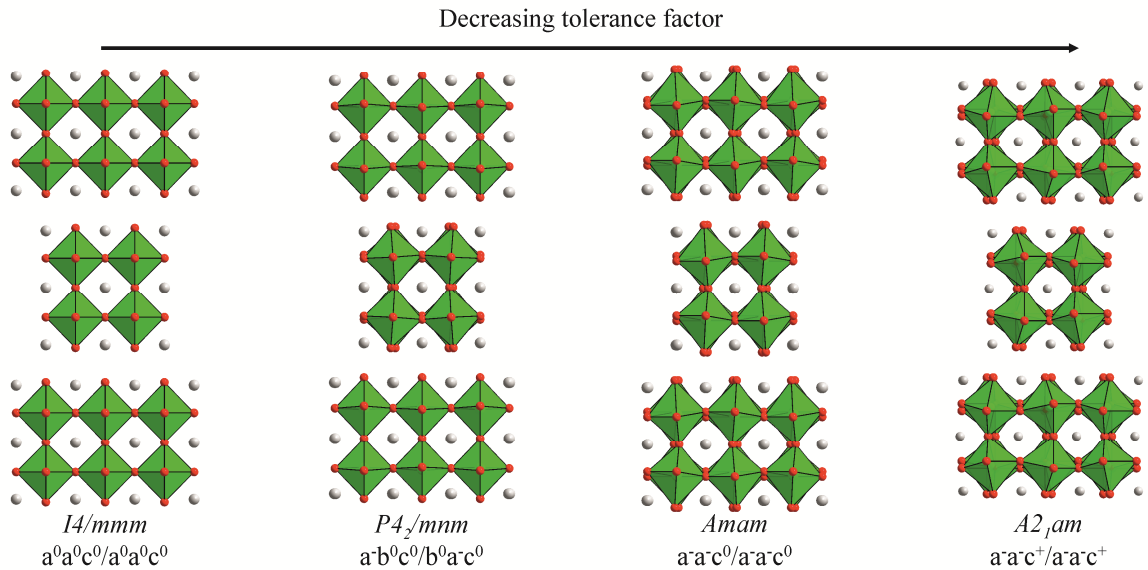
The cooperative tilting of the BO<sub>6</sub> units is driven by the relative sizes of the A- and B-cations (conveniently parameterized by the Goldschmidt tolerance factor,  $t = \langle A-O \rangle / \sqrt{2} \times \langle B-O \rangle$ )<sup>19</sup> and allows cation combinations with a wide range of radius ratios to form thermodynamically stable perovskite structures. A further important feature of these structural distortions is that they necessarily modify the lattice symmetry of the perovskite framework – a feature that can be utilized to break inversion symmetry.

Figure 1a shows a representation of a ‘GdFeO<sub>3</sub> distorted’ perovskite framework (the distortion is described as  $a^-a^+c^+$  in Glazer notation).<sup>20,21</sup> It can be seen that the collective rotations of the BO<sub>6</sub> units drive a coupled displacement of the A-cations to the ‘left’ and ‘right’ as indicated by arrows in Figure 1a. In the lattice shown, the direction of the A-cation displacement inverts between adjacent layers, so this structure is described

in the centrosymmetric space group  $Pnma$ . This reciprocal feature of the A-cation displacements means that in order to break inversion symmetry using this type of collective distortion, perovskite lattices with A-site or B-site cation order are required.<sup>22–25</sup> Unfortunately the preparation of cation ordered perovskite phases is also a significant synthetic challenge.

The need to prepare cation-ordered phases can be avoided by lowering the dimensionality of the lattice by switching to the layered variants of the perovskite structure which have two-dimensional arrays of apex-linked octahedra. While A<sub>2</sub>BO<sub>4</sub>  $n = 1$  Ruddlesden-Popper frameworks generally require A-cation order to break inversion symmetry,<sup>26,27</sup> the collective BO<sub>6</sub> rotations and A-cation displacements in A<sub>3</sub>B<sub>2</sub>O<sub>7</sub>,  $n = 2$  Ruddlesden-Popper phases can break inversion symmetry in the absence of cation order.<sup>28,29</sup> Figure 1b shows a representation of an  $n = 2$  Ruddlesden-Popper structure which adopts the same  $a^-a^+c^+ / a^-a^+c^+$  twisting distortion as the perovskite framework shown in Figure 1a (two sets of Glazer descriptors are required to describe the distortions of Ruddlesden-Popper phases as adjacent layers need not necessarily be distorted in the same way). The collective rotations of the BO<sub>6</sub> units in this layered framework lead to A-cation displacements analogous to those seen in the 3D perovskite framework, but now the layers of A-cations associated with each perovskite double layer are grouped into sets of three, so the A-cation displacements do not ‘cancel’ and inversion symmetry is broken, resulting in a network described in an acentric space group  $A2_1am$ . Ferroelectric behavior has recently been reported in (Ca,Sr)<sub>3</sub>Ti<sub>2</sub>O<sub>7</sub> by this mechanism.<sup>30</sup>

The prospect of preparing NCS phases in the absence of SOJT cations by utilizing the tilting distortions of  $n = 2$  Ruddlesden-Popper phases is clearly attractive. However, implementing these ideas in real materials is also challenging. This is because extremely small tolerance factors are required to stabilize the desired  $a^-a^+c^+ / a^-a^+c^+$ , ‘ $A2_1am$ ’ distorted framework. A recent study by Pitcher *et al.* examining the tilting distortions of Fe<sup>3+</sup> based  $n = 2$  Ruddlesden-Popper phases demonstrates this clearly.<sup>31</sup> Starting with La<sub>2</sub>BaFe<sub>2</sub>O<sub>7</sub>, which



**Figure 2.** The sequence of structural distortions which occur as the tolerance factor of  $n = 2$  Ruddlesden-Popper phases is reduced.

adopts an undistorted  $n = 2$  Ruddlesden-Popper structure (space group  $I4/mmm$ ), smaller cations were substituted onto the A-cation site to drive the framework to adopt increasingly distorted arrangements. Thus  $\text{Tb}_2\text{SrFe}_2\text{O}_7$  adopts a ' $P4_2/mnm$ ',  $a^-b^0c^0/a^0a^-c^0$  distortion and  $\text{Tb}_2\text{CaFe}_2\text{O}_7$  adopts an ' $Amam$ '  $a^-a^-c^0/a^0a^-c^0$  distortion, as shown in Figure 2. However it was not possible to drive the framework to adopt the desired ' $A2_1am$ ',  $a^-a^-c^+/a^0a^-c^+$  distortion by A-site substitution. Instead partial substitution of the B-site  $\text{Fe}^{3+}$  by  $\text{Ti}^{4+}$  (an SOJT cation) was required to achieve the  $A2_1am$ , NCS distortion. This suggests that the stabilization of the  $A2_1am$  polar distortion in phases containing small, paramagnetic transition metal B-cations (a necessary prerequisite for magnetoelectric behavior) will only be possible in a few exceptional cases.

Given these difficulties, we have sought to use topochemical manipulation to stabilize polar twisting distortions of Ruddlesden-Popper phases, specifically the extensive fluorine insertion chemistry of double-layered Ruddlesden-Popper oxide phases.<sup>32-38</sup> As shown in Figure 3, fluorine can be inserted into tetrahedral interstitial sites within the rock salt layers of the framework, which in the simplest cases converts an  $\text{A}_3\text{B}_2\text{O}_7$  oxide phase into an  $\text{A}_3\text{B}_2\text{O}_7\text{F}_2$  oxide-fluoride. In addition to oxidizing the transition metal B-cations, fluorine insertion can have a dramatic influence on the twisting distortions of the host Ruddlesden-Popper lattice. In particular, fluorination appears to modify the twisting of octahedra around the crystallographic  $z$ -axis. For example fluorination of  $\text{Sr}_3(\text{Mn}_{0.5}\text{Ru}_{0.5})_2\text{O}_7$  to  $\text{Sr}_3(\text{Mn}_{0.5}\text{Ru}_{0.5})_2\text{O}_7\text{F}_2$  drives a change from the aristotype  $a^-a^-c^0/a^0a^-c^0$ ,  $I4/mmm$  framework to a  $a^-a^-c^0/a^0a^-c^-$ ,  $Acaa$  distorted lattice.<sup>33</sup> Similarly fluorination of  $\text{Sr}_3\text{Ru}_2\text{O}_7$  drives a disordered twisting of the  $\text{RuO}_6$  octahedra around the  $z$ -axis to yield an  $a^-a^-c^+/a^0a^-c^+$  distorted structure for  $\text{Sr}_3\text{Ru}_2\text{O}_7\text{F}_2$ .<sup>32</sup> This suggests that topochemical fluorination could be used to introduce a ' $z$ -twist' to other  $n = 2$  Ruddlesden-Popper oxide phases and drive a phase with an  $a^-a^-c^0/a^0a^-c^0$ ,  $Amam$  distortion to adopt an  $a^-a^-c^+/a^0a^-c^+$ ,  $A2_1am$  polar structure. Here we describe the topochemical fluorination of  $\text{La}_3\text{Ni}_2\text{O}_7$ , an  $n = 2$  Ruddlesden-Popper phase which adopts an  $Amam$  distorted structure,<sup>39</sup> and contains an oxidizable transition metal cations, making it an ideal host phase to test this idea.

### Experimental

**Synthesis.**  $\text{La}_3\text{Ni}_2\text{O}_7$  was synthesized via a citrate method. Suitable stoichiometric ratios of  $\text{La}_2\text{O}_3$  (99.99%, dried at 900 °C) and Ni powder (99.99%) were dissolved in a minimal quantity of 6 M nitric acid. Citric acid and ethylene glycol were then added, and the solution was heated with constant stirring. The gels thus formed were heated to 350 °C until a loose black powder was obtained. The powder was ground and then heated to 1000 °C in air at a rate of 1 °C/min, to remove the remaining organic components. The resulting powder was then pressed into pellets before 2 further 48 h heating cycles at 1250 °C under flowing oxygen. X-ray powder diffraction data confirmed the formation of single phase samples, with lattice parameters in good agreement with previously reported values ( $a = 5.392(1)$  Å,  $b = 5.447(1)$  Å,  $c = 20.517(1)$  Å).<sup>39</sup>

Fluorination of  $\text{La}_3\text{Ni}_2\text{O}_7$  was carried out using  $\text{CuF}_2$  as a fluorination agent, in the same manner as has been described previously.<sup>32,36,40</sup> To avoid contamination of the samples with  $\text{CuO}$  which occurs when the fluorination agent is mixed

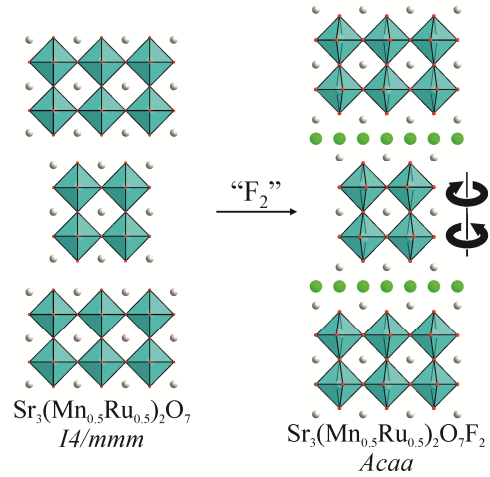


**Figure 3.** Topochemical fluorination of  $\text{Sr}_3(\text{Mn}_{0.5}\text{Ru}_{0.5})_2\text{O}_7$  to  $\text{Sr}_3(\text{Mn}_{0.5}\text{Ru}_{0.5})_2\text{O}_7\text{F}_2$  induces a ' $z$ -twist' into the  $n = 2$  Ruddlesden-Popper network.

directly into the sample, the  $\text{CuF}_2$  was heated separately from the sample at 500 °C under flowing oxygen to liberate fluorine. The resulting  $\text{O}_2/\text{F}_2$  gas mixture was then passed over a sample of  $\text{La}_3\text{Ni}_2\text{O}_7$  powder, held at 270 °C in adjacent furnace. Samples were treated in this way for two periods of 48 h, with the  $\text{CuF}_2$  reagent being replaced between heating periods. To improve the crystallinity of the fluorinated products, samples were finally heated in sealed, evacuated silica ampules at 350 °C for 48 h.

**Characterization.** X-ray powder diffraction data were collected using a PANalytical X'pert diffractometer incorporating an X'celerator position sensitive detector (monochromatic  $\text{Cu K}\alpha_1$  radiation). Neutron powder diffraction data were collected from a sample contained within a vanadium can, using the POLARIS diffractometer (ISIS neutron source, U.K). Rietveld profile refinement was performed using the GSAS suite of programs.<sup>41</sup> Magnetization data were collected using a Quantum Design MPMS SQUID magnetometer. Average nickel oxidation states were determined by iodometric titration. Titrations were performed by dissolving samples in a dilute HCl solution containing an excess of KI and titrating the amount of liberated  $\text{I}_2$  with standardized  $\text{Na}_2\text{S}_2\text{O}_3$  solution. Thermogravimetric data were collected by heating powder samples under a 10%  $\text{H}_2$  in  $\text{N}_2$  atmosphere on a Mettler-Toledo MX1 thermogravimetric microbalance.

### Results

Heating samples of  $\text{La}_3\text{Ni}_2\text{O}_7$  at 270 °C under the fluorination conditions described above, led to an expansion in the  $c$ -lattice parameter of the material, and ultimately the formation of an orthorhombic phase ( $a = 5.431$  Å  $b = 5.507$  Å,  $c = 22.48$  Å) consistent with the formation of a topochemically fluorinated compound of composition  $\text{La}_3\text{Ni}_2\text{O}_x\text{F}_y$ .

**Chemical characterization.** Crystallographic characterization of the  $\text{La}_3\text{Ni}_2\text{O}_x\text{F}_y$  phase, described below, indicated that all anion sites were fully occupied and thus  $x + y = 9$ , as observed for other fluorinated  $n = 2$  Ruddlesden-Popper phases.<sup>32,33,36,37</sup> This information, combined with iodometric titration results, indicated an average nickel oxidation state of

$\text{Ni}^{+2.75}$ , consistent with a chemical formula of  $\text{La}_3\text{Ni}_2\text{O}_{5.5}\text{F}_{3.5}$ .

Thermogravimetric data collected during the reduction of  $\text{La}_3\text{Ni}_2\text{O}_x\text{F}_y$  indicated a mass loss of 6.4% (Supporting Information) as the sample was converted to a mixture of Ni,  $\text{La}_2\text{O}_3$  and  $\text{LaF}_3$ . This is also consistent with an initial composition of  $\text{La}_3\text{Ni}_2\text{O}_{5.5}\text{F}_{3.5}$ .

**Structural characterization.** Neutron powder diffraction data collected from  $\text{La}_3\text{Ni}_2\text{O}_{5.5}\text{F}_{3.5}$  could be indexed using an orthorhombic unit cell, which on initial inspection appeared to have extinction conditions consistent with A-centering. Considering these observations, and the symmetry analysis of the twisting distortions of  $n = 2$  Ruddlesden-Popper phases by Aleksandrov and Bartolome,<sup>42</sup> three structural models were constructed to describe  $\text{La}_3\text{Ni}_2\text{O}_{5.5}\text{F}_{3.5}$ , each based on a fluorine-inserted  $n = 2$  Ruddlesden-Popper structure, but with a different set of cooperative octahedral tilting distortions: a model in space group  $Amam$  with the  $a^-a^-c^0/a^-a^-c^0$  distortion of the  $\text{La}_3\text{Ni}_2\text{O}_7$  parent phase;<sup>39</sup> a model in space group  $A2/a$  with the  $a^-a^-c^0/a^-a^-c^0$  distortion of  $\text{La}_2\text{SrCr}_2\text{O}_7\text{F}_2$ ;<sup>36</sup> a model in space group  $A2_1am$  with a polar  $a^-a^-c^+/a^-a^-c^+$  distortion.

Refinement of these three models against the neutron powder diffraction data proceeded smoothly. All atomic positional and displacement parameters were refined freely. Given the very similar neutron scattering cross sections of oxide and fluoride ( $\text{O} = 5.80 \text{ fm}$ ;  $\text{F} = 5.65 \text{ fm}$ )<sup>43</sup> no attempt was made to differentiate between the two anions at this stage, with all anion sites treated as if they were occupied by oxide.

Fitting statistics for the three structural models (Table 1) reveal that the fit to the data by the model in space group  $Amam$  is significantly worse than the fits using models in space groups  $A2_1am$  and  $A2/a$ , and so the  $Amam$  model was eliminated from consideration. The two remaining models, described in space groups  $A2_1am$  and  $A2/a$ , only differ by the ‘sense’ in which the  $\text{Ni}(\text{O/F})_6$  octahedra are rotated around the  $z$ -axis – ‘in-phase’ for the  $A2_1am$  model ( $c^+$ ), ‘out of phase’ for the  $A2/a$  model ( $c^-$ ). However, despite this significant structural difference, the fitting statistics for the two models are almost identical (Table 1). This suggests that neither the  $A2_1am$  nor the  $A2/a$  model are describing the  $z$ -axis tilts of the  $\text{Ni}(\text{O/F})_6$  octahedra of  $\text{La}_3\text{Ni}_2\text{O}_{5.5}\text{F}_{3.5}$  correctly, but given the poor fit using the  $Amam$  model this is not simply because the  $z$ -tilt is zero. Instead this suggests the  $z$ -axis tilts are arranged in a more complex manner.

Close inspection of the fits to the neutron diffraction data using the  $A2_1am$  and  $A2/a$  models suggest that the A-centering extinction conditions, which were initially thought to apply, are violated by a few weak diffraction features. This is clearest in the  $d$ -spacing range  $2.2 < d/\text{\AA} < 2.5$  as shown in Figure 4. The symmetry analysis by Aleksandrov and Bartolome<sup>42</sup> shows that the lifting of the A-centering of the lattice is consistent with a structural model in the primitive space group  $Pnam$  which describes an  $a^-a^-c^+/a^-a^-(c^+)$  cooperative distortion in which the  $z$ -axis tilts of the octahedra are ‘in-phase’ in each perovskite slab, but the direction of the rotation inverts between neighboring slabs to yield a centrosymmetric lattice. The body centering of adjacent double perovskite blocks within the aristotype  $n = 2$  Ruddlesden-Popper structure complicates the description of the relative phase of the  $(a^-a^-c^0)$  and  $(a^0a^0c^+)$  tilts in adjacent layers. A detailed symmetry analysis highlighting why the sense in which tilts are combined in an

$a^-a^-c^+/a^-a^-(c^+)$   $A2_1am$  and an  $a^-a^-c^+/a^-a^-(c^+)$   $Pnam$  phase only leads to global breaking of inversion symmetry in the former case, is given in the Supporting Information, and has also been discussed in detail by others.<sup>44</sup>

Refinement of this primitive model proceeded smoothly, to give a much improved fit to the data, both statistically (Table 1) and visually (Figure 4). Full details of the refined structure of  $\text{La}_3\text{Ni}_2\text{O}_{5.5}\text{F}_{3.5}$  are given in Table 2, with selected bond lengths and angles in Table 3. A plot of the full fit to the data is shown in the Supporting Information. A representation of the structure of  $\text{La}_3\text{Ni}_2\text{O}_{5.5}\text{F}_{3.5}$  is shown in Figure 5.

Space Group	Glazer Tilt	No. of variables	$\chi^2$	wRp(%)	Rp(%)
$Amam$	$a^-a^-c^0/a^-a^-c^0$	91	5.002	4.60	6.05
$A2/a$	$a^-a^-c^-/a^-a^-c^-$	101	4.096	4.16	5.75
$A2_1am$	$a^-a^-c^+/a^-a^-c^+$	101	3.965	4.11	5.89
$Pnam$	$a^-a^-c^+/a^-a^-(c^+)$	102	2.563	3.25	4.16

**Table 1.** Fitting statistics from the structural refinement of  $\text{La}_3\text{Ni}_2\text{O}_{5.5}\text{F}_{3.5}$ .

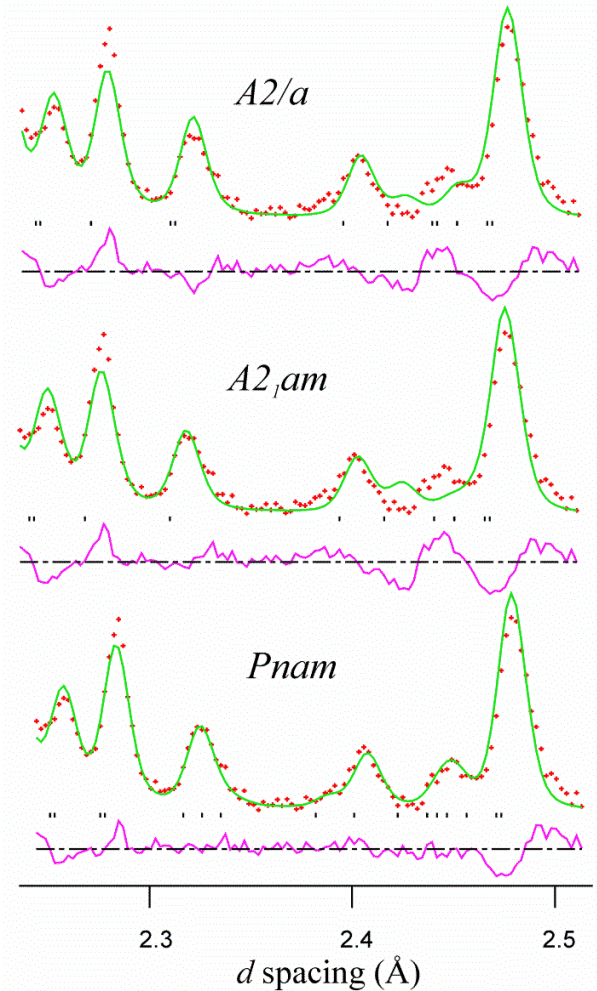


**Figure 4.** Observed, calculated and difference plots comparing the fits to the data using structural models in space groups  $A2/a$ ,  $A2_1am$  and  $Pnam$ .



Atom	x	y	z	U <sub>iso</sub> (Å <sup>2</sup> )
La(1)	0.7148(7)	0.0017(9)	¼	0.0059(6)
La(2)	0.7564(6)	0.9956(6)	0.0758(1)	0.0060(4)
Ni(1)	0.7615(5)	0.0036(5)	0.8353(1)	0.0030(2)
O(1)	0.7335(11)	0.5687(7)	¼	0.0034(7)
O/F(2)	0.7727(8)	0.9446(6)	0.9198(1)	0.0072(6)
O(3)	0.9868(8)	0.2755(7)	0.8524(1)	0.0057(5)
O(4)	0.4501(8)	0.2816(8)	0.3278(1)	0.0107(7)
F(5)	0.9917(8)	0.2557(9)	0.9925(1)	0.0075(6)
<p>La<sub>3</sub>Ni<sub>2</sub>O<sub>5.5</sub>F<sub>3.5</sub> - space group: <i>Pnam</i>  <math>a = 5.431(1)</math> Å <math>b = 5.507(1)</math> Å <math>c = 22.483(4)</math> Å  Volume = 672.5(4) Å<sup>3</sup>  <math>\chi^2 = 2.563</math>; <math>wRp = 3.25\%</math>; <math>Rp = 4.16\%</math>.</p>				

**Table 2.** Parameters from the structural refinement of La<sub>3</sub>Ni<sub>2</sub>O<sub>5.5</sub>F<sub>3.5</sub> against neutron powder diffraction data collected at 298 K. Anion site O/F(2) has a 25%:75% oxide: fluoride occupation.

	La <sub>3</sub> Ni <sub>2</sub> O <sub>7</sub>	La <sub>3</sub> Ni <sub>2</sub> O <sub>5.5</sub> F <sub>3.5</sub>
	Bond length (Å)	Bond length (Å)
Ni-O1	1.975(2)	1.951(2)
Ni-O2	2.227(5)	1.928(3)
Ni-O3	1.906(2)	1.963(5)
		1.972(5)
Ni-O4	1.941(2)	1.954(5)
		1.994(5)
	Bond angle (°)	Bond angle (°)
Ni-O1-Ni	167.64(8)	158.76(26)
Ni-O3-Ni	169.21(1)	154.71(26)
Ni-O4-Ni	171.14(1)	161.39(27)
	Octahedron rotation angle (°)	Octahedron rotation angle (°)
x-axis	4.91(7)	8.10(10)
y-axis	4.91(7)	8.10(10)
z-axis	0	6.85(7)

**Table 3.** Selected bond lengths and angles from refined structures of La<sub>3</sub>Ni<sub>2</sub>O<sub>5.5</sub>F<sub>3.5</sub> and La<sub>3</sub>Ni<sub>2</sub>O<sub>7</sub> at 298 K.

**Magnetic Characterization.** Magnetization data collected from La<sub>3</sub>Ni<sub>2</sub>O<sub>5.5</sub>F<sub>3.5</sub> in an applied field of 100 Oe, show weak divergence between zero-field cooled and field cooled data sets below  $T \sim 50$  K, as shown in Figure 6. Despite this feature, the zero-field cooled data can be approximately fitted to the Curie-Weiss law over the whole  $5 < T/K < 300$  temperature range to yield values of  $C = 0.142(3)$  cm<sup>3</sup> K mol<sup>-1</sup>,  $\theta = -14.4(2)$  K. The low value of the Curie constant, combined with the weak divergence between zero-field cooled and field cooled data suggest the localized spins on the nickel centers

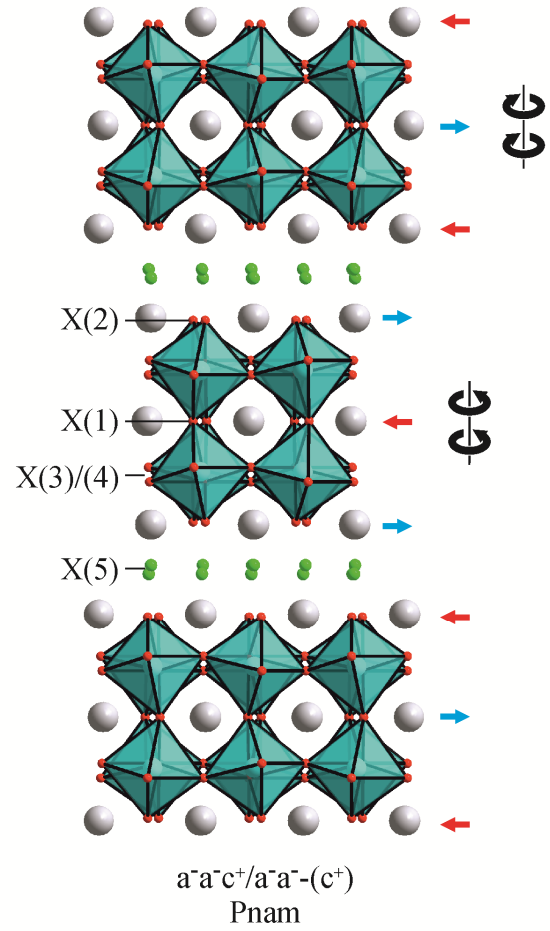


**Figure 5.** The refined structure of La<sub>3</sub>Ni<sub>2</sub>O<sub>5.5</sub>F<sub>3.5</sub> viewed along the [110] axis. Blue and green spheres represent lanthanum and nickel cations respectively, red and green spheres represent anion positions.

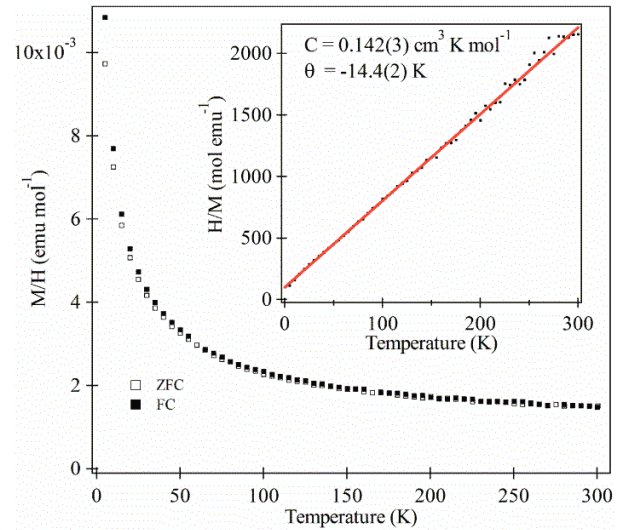


**Figure 6.** Zero-field cooled and field-cooled magnetization data collected as a function of temperature from La<sub>3</sub>Ni<sub>2</sub>O<sub>5.5</sub>F<sub>3.5</sub> in an applied field of 100 Oe.

are not behaving as simple paramagnetic moments. However neutron powder diffraction data collected from  $\text{La}_3\text{Ni}_2\text{O}_{5.5}\text{F}_{3.5}$  at 5 K can be readily fitted by the same structural model as used for the 300 K data, and show no indication of magnetic order.

### Discussion

Heating  $\text{La}_3\text{Ni}_2\text{O}_7$  under an  $\text{F}_2/\text{O}_2$  flow leads to the formation of  $\text{La}_3\text{Ni}_2\text{O}_{5.5}\text{F}_{3.5}$  via a topochemical anion insertion/exchange reaction. The relatively high level of fluoride-for-oxide anion exchange means that the average nickel oxidation state only rises from  $\text{Ni}^{+2.5}$  to  $\text{Ni}^{+2.75}$  on fluorination, rather than rising to the value of  $\text{Ni}^{+3.5}$  expected for the hypothetical ‘insertion only’ product,  $\text{La}_3\text{Ni}_2\text{O}_7\text{F}_2$ . Similar high levels of anion exchange have been observed during the fluorination of iron-containing  $n = 2$  Ruddlesden-Popper phases, such as the formation of  $\text{Sr}_3(\text{Fe}_{0.5}\text{Ru}_{0.5})_2\text{O}_{5.5}\text{F}_{3.5}$  from  $\text{Sr}_3(\text{Fe}_{0.5}\text{Ru}_{0.5})_2\text{O}_7$  or the preparation of  $\text{La}_2\text{BaFe}_2\text{O}_5\text{F}_4$  from  $\text{La}_2\text{BaFe}_2\text{O}_7$ .<sup>33,37</sup> In this instance the high level of anion substitution during the fluorination of  $\text{La}_3\text{Ni}_2\text{O}_7$  can be attributed to the difficulty of stabilizing the  $\text{Ni}^{3+}$  oxidation state.

As noted above, the poor X-ray and neutron scattering contrast between  $\text{F}^-$  and  $\text{O}^{2-}$  makes it impossible to determine the anion distribution in oxide-fluoride phases directly. However it is possible in some cases to deduce the oxide/fluoride distribution by close examination of the local anion bonding environment through the use of bond valence sums. This approach has proved particularly effective for fluorinated  $n = 2$  Ruddlesden-Popper phases.<sup>33,36</sup>

Table 4 lists the bond valence sums (BVS) for the 5 crystallographically distinct anion sites in the structure of  $\text{La}_3\text{Ni}_2\text{O}_{5.5}\text{F}_{3.5}$ , calculated on the basis of occupation by oxide or fluoride, and the corresponding anions sites in the structure of  $\text{La}_3\text{Ni}_2\text{O}_7$  calculated for oxide occupation. The anion site labelling scheme is shown in Figure 5. BVS values calculated for the ‘new’ tetrahedral anion site X(5), which resides in the rock salt layers of the extended structure, are the lowest of any of the 5 anion sites and consistent with occupation by fluoride ions rather than oxide ions. Occupation of these ‘interstitial’ anion sites exclusively by fluoride ions has been observed widely in other topochemically fluorinated  $n = 2$  Ruddlesden-Popper oxide phases.<sup>32,33,36,37</sup>

The anion stoichiometry of  $\text{La}_3\text{Ni}_2\text{O}_{5.5}\text{F}_{3.5}$  indicates that fluoride ions must reside on other anion sites, in addition to the X(5) site. Table 4 reveals that the BVS of the X(2) ‘apical’ anion site is significantly lower than the remaining anion sites in the structure of  $\text{La}_3\text{Ni}_2\text{O}_{5.5}\text{F}_{3.5}$ , suggesting the remaining fluoride ions are located here, resulting in a 75%  $\text{F}^-$ :25%  $\text{O}^{2-}$  occupation, as indicated in Table 2. Again there is precedent for the preferred fluoride-for-oxide anion exchange at this apical anion site as a similar anion distribution is observed in the structure of  $\text{Sr}_3(\text{Fe}_{0.5}\text{Ru}_{0.5})_2\text{O}_{5.5}\text{F}_{3.5}$ .<sup>33</sup>

As shown in Table 3, the insertion/exchange of fluorine into  $\text{La}_3\text{Ni}_2\text{O}_7$  to form  $\text{La}_3\text{Ni}_2\text{O}_{5.5}\text{F}_{3.5}$  leads to a tightening of all the Ni-X-Ni bond angles. Separating the rotations of the  $\text{NiX}_6$  octahedra in the two phases into component rotations around the Cartesian axes, reveals that on fluorination the rotational distortions around all three axes increase, from  $4.91(7)^\circ$  to  $8.1(1)^\circ$  around the x- and y-axes, and from zero to  $6.85(7)^\circ$  around the z-axis.

$\text{La}_3\text{Ni}_2\text{O}_7$		$\text{La}_3\text{Ni}_2\text{O}_{5.5}\text{F}_{3.5}$		
Anion	BVS (O)	Anion	BVS (O)	BVS (F)
O(1)	1.840	X(1),O(1)	1.974	1.563
O(2)	1.706	X(2), O/F(2)	1.481	1.147
O(3)	2.107	X(3),O(3)	1.918	1.516
O(4)	2.017	X(4),O(4)	1.811	1.436
		X(5),F(5)	1.404	1.029

**Table 4.** Anion bond valence sums from  $\text{La}_3\text{Ni}_2\text{O}_7$  and  $\text{La}_3\text{Ni}_2\text{O}_{5.5}\text{F}_{3.5}$ .

The tightening of all the Ni-X-Ni bond angles on fluorination can be attributed to a compression of the perovskite double layers along the z-axis. The  $\text{NiO}_6$  octahedra present in  $\text{La}_3\text{Ni}_2\text{O}_7$  have a large axial distortion, such that the ratio of  $\text{Ni-O}_{\text{axial}}/\text{Ni-O}_{\text{equatorial}} = 1.09$ . Insertion of fluoride leads to a compression of the perovskite layers along the z-axis, presumably due to enhanced anion-anion repulsions, resulting in the  $\text{Ni}(\text{O}/\text{F})_6$  octahedra in  $\text{La}_3\text{Ni}_2\text{O}_{5.5}\text{F}_{3.5}$  being axially compressed ( $\text{Ni-X}_{\text{axial}}/\text{Ni-X}_{\text{equatorial}} = 0.98$ ). This transformation from ‘tall-thin’  $\text{NiO}_6$  to ‘short-fat’  $\text{Ni}(\text{O}/\text{F})_6$  naturally leads to an expansion of the Ni-X equatorial bonds, and introduces a rotation around the z-axis to accommodate these longer bonds within the perovskite framework (despite a slight expansion in the *a* and *b* lattice parameters).

The introduction of an in-phase z-twist to the network of octahedra results in each perovskite double layer adopting an  $a^-c^+$  distortion pattern, which lifts the inversion symmetry of each layer via the coupled displacements of the lanthanum A-cations. However despite breaking the inversion symmetry of the Ruddlesden-Popper framework locally, this distortion does not break the inversion symmetry globally because the ‘sense’ of the in-phase z-axis rotation inverts between adjacent perovskite layers, and as a result the direction of the A-cation displacements is also inverted between adjacent perovskite layers. Thus the framework is described in the centrosymmetric space group *Pnam*, not the polar space group *A2<sub>1</sub>am*. To our knowledge this is the first report of an  $n = 2$  Ruddlesden-Popper oxide, or derived phase, adopting this ‘*Pnam*’ distortion, however analogous anti-polar distorted structures have been suggested as intermediates in the switching of polar *A2<sub>1</sub>am* phases.<sup>44</sup>

The recovery of global inversion symmetry via the anti-alignment of locally acentric units (in this instance the polar perovskite double-layers) is an issue which has long hampered the design and synthesis of NCS phases. This has been particularly apparent when a basic building unit (BBU) approach has been adopted to prepare NCS phases. The BBU approach involves crystalizing acentric units, such as metal oxide-fluoride complex anions ( $\text{NbOF}_5^{2-}$ ,  $\text{VOF}_5^{2-}$ ,  $\text{MoO}_2\text{F}_4^{2-}$ , etc)<sup>45-47</sup> into extended networks with the intention of forming NCS lattices. However it has been widely observed that centrosymmetric structures in which the BBUs anti-align, or adopt orientationally disordered arrangements, tend to be favored unless specific steps are taken to oppose this. In the oxide-fluoride case, the use of particular bridging ligands<sup>48,49</sup> or specific structure directing interactions between the oxide-fluoride anions and charge balancing cations<sup>50</sup> can be used to

suppress the adoption of centrosymmetric lattices and direct the formation of NCS phases. This provides some hope that similar interactions can be employed within topochemically fluorinated Ruddlesden-Popper phases to suppress the formation of anti-ferroelectric structures and allow the formation of ferroelectric materials and by extension multiferroic materials.

### Conclusion

Topochemical fluorination of the  $n = 2$  Ruddlesden-Popper oxide  $\text{La}_3\text{Ni}_2\text{O}_7$  yields the oxide-fluoride  $\text{La}_3\text{Ni}_2\text{O}_{5.5}\text{F}_{3.5}$ . Insertion/exchange of fluoride ions leads to an enhancement of the structural distortion exhibited by the oxide starting material, driving a change from an  $A\text{mam}$ ,  $a\bar{a}c^0/a\bar{a}c^0$  lattice distortion to a  $P\text{nam}$   $a\bar{a}c^+/a\bar{a}(c^+)$  lattice distortion in the oxide-fluoride phase. The introduction of a cooperative octahedral tilt around the crystallographic  $z$ -axis leads to a local breaking of the inversion symmetry of the host lattice on fluorination, although the global inversion symmetry of the lattice is retained due to an alternation in the  $z$ -tilt direction in adjacent perovskite sheets.

In a wider context this study reaffirms previous observations that topochemical fluorination acts to enhance the titling and twisting distortions of  $n = 2$  Ruddlesden-Popper phases,<sup>32,33,36</sup> and as a result offers an alternative route, in addition to adjusting the tolerance factor by cation substitution, to tune the cooperative structural distortions of materials with this structure type. If appropriate methods can be found to suppress the formation of anti-ferroelectric phases, this facility to modify the structural distortions of layered perovskites will be particularly valuable in the directed search for magnetoelectric multiferroic materials, where the requirement to have paramagnetic centers necessitates the inclusion of transition metal B-cations with small ionic radii, which limits the minimum value the structural tolerance factor can take, and effectively precludes the stabilization of the highly-distorted frameworks required to break structural inversion symmetry.

### ASSOCIATED CONTENT

#### Supporting Information

Thermogravimetric data collected from  $\text{La}_3\text{Ni}_2\text{O}_{5.5}\text{F}_{3.5}$  under a 10:90  $\text{H}_2:\text{N}_2$  atmosphere; Observed calculated and difference plots from the structural refinement of  $\text{La}_3\text{Ni}_2\text{O}_{5.5}\text{F}_{3.5}$  against neutron powder diffraction data collected at 300 K; Comparison of octahedral rotations and A-cation displacements of  $A\text{mam}$ ,  $A2_1\text{am}$  and  $P\text{nam}$  distorted  $\text{A}_3\text{B}_2\text{O}_7\text{F}_2$  phases; Symmetry Analysis of the  $P\text{nam}$  Phase; Representation of  $\text{NiO}_6$  octahedra in  $A2_1\text{am}$  and  $P\text{nam}$  distorted phases superimposed. This material is available free of charge via the Internet at <http://pubs.acs.org>. This material for publication, refer to the journal's Instructions for Authors.

### AUTHOR INFORMATION

#### Corresponding Author

\* [michael.hayward@chem.ox.ac.uk](mailto:michael.hayward@chem.ox.ac.uk)

#### Author Contributions

The manuscript was written through contributions of all authors.

### ACKNOWLEDGMENT

We thank R. Smith for assistance collecting neutron powder diffraction data. Experiments at the ISIS pulsed neutron facility were supported by a beam time allocation from the Science and Technology Facilities Council. We thank SCG Chemicals Co. Ltd, Thailand for financial support. M.S.S. thanks the Royal Commission for the Exhibition of 1851 for a fellowship.

### REFERENCES

- (1) Goodenough, J. B. *Magnetism and the Chemical Bond*; Wiley: New York, 1963.
- (2) Blundell, S. *Magnetism in Condensed Matter*; Oxford University Press, 2001.
- (3) Spaldin, N. A. *Magnetic materials: fundamentals and applications*; 2nd ed.; Cambridge University Press, 2011.
- (4) Lines, M. E.; Glass, A. M. *Principles and Applications of Ferroelectrics and Related Materials*; Oxford University Press: Oxford, 1991.
- (5) Nye, F. J. *Physical Properties of Crystals*; Oxford University Press: Oxford, UK, 1957.
- (6) Cohen, R. E. Origin of Ferroelectricity in Perovskite Oxides. *Nature* **1992**, 358, 136.
- (7) Kang, S. K.; Tang, H.; Albright, T. A. Structures for D(0) Ml(6) and Ml(5) Complexes. *J. Am. Chem. Soc.* **1993**, 115, 1971.
- (8) Kunz, M.; Brown, I. D. Out-of-Center Distortions around Octahedrally Coordinated d(0) Transition-Metals. *J. Solid State Chem.* **1995**, 115, 395.
- (9) Pearson, R. G. The 2nd-Order Jahn-Teller Effect. *Theochem-Journal of Molecular Structure* **1983**, 12, 25.
- (10) Wheeler, R. A.; Whangbo, M. H.; Hughbanks, T.; Hoffmann, R.; Burdett, J. K.; Albright, T. A. Symmetrical Vs Asymmetric Linear M-X-M Linkages in Molecules, Polymers, and Extended Networks. *J. Am. Chem. Soc.* **1986**, 108, 2222.
- (11) Lefebvre, I.; Lannoo, M.; Allan, G.; Ibanez, A.; Fourcade, J.; Jumas, J. C.; Bearepaire, E. Electronic-Properties of Antimony Chalcogenides. *Phys. Rev. Lett.* **1987**, 59, 2471.
- (12) Lefebvre, I.; Szymanski, M. A.; Olivier-Fourcade, J.; Jumas, J. C. Electronic Structure of Tin Monochalcogenides from  $\text{SnO}$  to  $\text{SnTe}$ . *Phys. Rev. B* **1998**, 58, 1896.
- (13) Seshadri, R.; Hill, N. A. Visualizing the Role of Bi 6s "Lone Pairs" in the Off-Center Distortion in Ferromagnetic  $\text{BiMnO}_3$ . *Chem. Mater.* **2001**, 13, 2892.
- (14) Stoltzfus, M. W.; Woodward, P. M.; Seshadri, R.; Klepeis, J. H.; Bursten, B. Structure and Bonding in  $\text{SnWO}_4$ ,  $\text{PbWO}_4$ , and  $\text{BiVO}_4$ : Lone Pairs vs Inert Pairs. *Inorg. Chem.* **2007**, 46, 3839.
- (15) Watson, G. W.; Parker, S. C. Origin of the Lone Pair of  $\alpha\text{-PbO}$  from Density Functional Theory Calculations. *J. Phys. Chem. B* **1999**, 103, 1258.
- (16) Watson, G. W.; Parker, S. C.; Kresse, G. Ab Initio Calculation of the Origin of the Distortion of  $\alpha\text{-PbO}$ . *Phys. Rev. B* **1999**, 59, 8481.
- (17) Hill, N. A. Why Are There So Few Magnetic Ferroelectrics. *J. Phys. Chem. B* **2000**, 104, 6694.
- (18) Benedek, N. A.; Rondinelli, J. M.; Djani, H.; Ghosez, P.; Lightfoot, P. Understanding Ferroelectricity in Layered Perovskites: New Ideas and Insights From Theory and Experiments. *Dalton Trans.* **2015**, 44, 10543.
- (19) Goldschmidt, V. M. *Naturwissenschaften* **1926**, 14, 477.
- (20) Glazer, A. M. Classification of tilted Octahedra in Perovskites. *Acta Crystallogr. Sect. B-Struct. Commun.* **1972**, B 28, 3384.
- (21) Woodward, P. M. Octahedral Tilting in Perovskites .1. Geometrical Considerations. *Acta Crystallogr. Sect. B-Struct. Commun.* **1997**, 53, 32.
- (22) Rondinelli, J. M.; Fennie, C. J. Octahedral Rotation-Induced Ferroelectricity in Cation Ordered Perovskites. *Adv. Mater.* **2012**, 24, 1961.

- (23) Knapp, M. C.; Woodward, P. M. A-site Cation Ordering in AA'BB'O6 Perovskites. *J. Solid State Chem.* **2006**, *179*, 1076.
- (24) King, G.; Woodward, P. M. Cation Ordering in Perovskites. *J. Mater. Chem.* **2010**, *20*, 5785.
- (25) Bousquet, E.; Dawber, M.; Stucki, N.; Lichtensteiger, C.; Hermet, P.; Gariglio, S.; Triscone, J. M.; Ghosez, P. Improper Ferroelectricity in Perovskite Oxide Artificial Superlattices. *Nature* **2008**, *452*, 732.
- (26) Akamatsu, H.; Fujita, K.; Kuge, T.; Sen Gupta, A.; Togo, A.; Lei, S. M.; Xue, F.; Stone, G.; Rondinelli, J. M.; Chen, L. Q.; Tanaka, I.; Gopalan, V.; Tanaka, K. Inversion Symmetry Breaking by Oxygen Octahedral Rotations in the Ruddlesden-Popper NaRTiO<sub>4</sub> Family. *Phys. Rev. Lett.* **2014**, *112*.
- (27) Cammarata, A.; Rondinelli, J. M. Ferroelectricity from coupled cooperative Jahn-Teller distortions and octahedral rotations in ordered Ruddlesden-Popper manganates. *Phys. Rev. B* **2015**, *92*, 14102.
- (28) Benedek, N. A.; Fennie, C. J. Hybrid Improper Ferroelectricity: A Mechanism for Controllable Polarization-Magnetization Coupling. *Phys. Rev. Lett.* **2011**, *106*, 107204.
- (29) Mulder, A. T.; Benedek, N. A.; Rondinelli, J. M.; Fennie, C. J. Turning ABO<sub>3</sub> Antiferroelectrics into Ferroelectrics: Design Rules for Practical Rotation-Driven Ferroelectricity in Double Perovskites and A<sub>3</sub>B<sub>2</sub>O<sub>7</sub> Ruddlesden-Popper Compounds. *Advanced Functional Materials* **2013**, *23*, 4810.
- (30) Oh, Y. S.; Luo, X.; Huang, F. T.; Wang, Y. Z.; Cheong, S. W. Experimental demonstration of hybrid improper ferroelectricity and the presence of abundant charged walls in (Ca, Sr)<sub>3</sub>Ti<sub>2</sub>O<sub>7</sub> crystals. *Nat. Mater.* **2015**, *14*, 407.
- (31) Pitcher, M. J.; Mandal, P.; Dyer, M. S.; Alaria, J.; Borisov, P.; Niu, H.; Claridge, J. B.; Rosseinsky, M. J. Tilt Engineering of Spontaneous Polarization and Magnetization Above 300 K in a Bulk Layered Perovskite. *Science* **2015**, *347*, 420.
- (32) Li, R. K.; Greaves, C. Double-Layered Ruthenate Sr<sub>3</sub>Ru<sub>2</sub>O<sub>7</sub>F<sub>2</sub> Formed by Fluorine Insertion into Sr<sub>3</sub>Ru<sub>2</sub>O<sub>7</sub>. *Phys. Rev. B* **2000**, *62*, 3811.
- (33) Denis Romero, F.; Bingham, P. A.; Forder, S. D.; Hayward, M. A. Topochemical Fluorination of Sr<sub>3</sub>(M<sub>0.5</sub>Ru<sub>0.5</sub>)<sub>2</sub>O<sub>7</sub> (M = Ti, Mn, Fe) n = 2 Ruddlesden-Popper Phases. *Inorg. Chem.* **2013**, *52*, 3388.
- (34) Sivakumar, T.; Wiley, J. B. Topotactic Route for New Layered Perovskite Oxide Containing Fluorine. *Mater. Res. Bull.* **2009**, *44*, 74.
- (35) Hayward, M. A. Topochemical Reactions of Layered Transition-Metal Oxides. *Semiconductor Science and Technology* **2014**, *29*, 64010.
- (36) Zhang, R.; Read, G.; Lang, F.; Lancaster, T.; Blundell, S. J.; Hayward, M. A. La<sub>2</sub>SrCr<sub>2</sub>O<sub>7</sub>F<sub>2</sub> - A Ruddlesden-Popper Oxyfluoride Containing Octahedrally Coordinated Cr<sup>4+</sup> Centers. *Inorg. Chem.* **2016**, *55*, 3169.
- (37) Gurusinghe, N. N. M.; Fones, J. C.; Marco, J. F.; Berry, F. J.; Greaves, C. Fluorine Insertion into the Ruddlesden-Popper Phase La<sub>2</sub>BaFe<sub>2</sub>O<sub>7</sub>: The Structure and Magnetic Properties of La<sub>2</sub>BaFe<sub>2</sub>O<sub>5</sub>F<sub>4</sub>. *Dalton Trans.* **2014**, *43*, 2038.
- (38) Hayward, M. A. In *Comprehensive Inorganic Chemistry II*; Reedijk, J., Poeppelmeier, K. R., Eds.; Elsevier: Oxford, 2013; Vol. 2, p 417.
- (39) Ling, C. D.; Argyriou, D. N.; Wu, G. Q.; Neumeier, J. J. Neutron Diffraction Study of La<sub>2</sub>Ni<sub>2</sub>O<sub>7</sub>: Structural Relationships Among n=1, 2, and 3 Phases La<sub>n+1</sub>NiO<sub>3n+1</sub>. *J. Solid State Chem.* **2000**, *152*, 517.
- (40) Luo, K.; Tran, T. T.; Halasyamani, P. S.; Hayward, M. A. Synthesis and Selective Topochemical Fluorination of the Cation and Anion-Vacancy Ordered Phases Ba<sub>2</sub>YCoO<sub>5</sub> and Ba<sub>3</sub>YCo<sub>2</sub>O<sub>7.5</sub>. *Inorg. Chem.* **2013**, *52*, 13762.
- (41) Larson, A. C.; Von Dreele, R. B.; Los Alamos National Laboratory Report LAUR 86-748: 2000.
- (42) Aleksandrov, K. S.; Bartolome, J. Octahedral Tilt Phases in Perovskite-like Crystals with Slabs Containing an Even Number of Octahedral Layers. *J. Phys.:Condens. Matter* **1994**, *6*, 8219.
- (43) Sears, V. F. Neutron Scattering Lengths and Cross Sections. *Neutron News* **1992**, *3*, 26.
- (44) Nowadnick, E. A.; Fennie, C. J. Domains and ferroelectric switching pathways in Ca<sub>3</sub>Ti<sub>2</sub>O<sub>7</sub> from first principles. *Phys. Rev. B* **2016**, *94*, 104105.
- (45) Izumi, H. K.; Kirsch, J. E.; Stern, C. L.; Poeppelmeier, K. R. Examining the Out-of-Center Distortion in the [NbOF<sub>5</sub>](<sup>2-</sup>) Anion. *Inorg. Chem.* **2005**, *44*, 884.
- (46) Welk, M. E.; Norquist, A. J.; Stern, C. L.; Poeppelmeier, K. R. The Structure-Directing Properties of VOF<sub>5</sub> (<sup>2-</sup>). *Inorg. Chem.* **2000**, *39*, 3946.
- (47) Heier, K. R.; Norquist, A. J.; Halasyamani, P. S.; Duarte, A.; Stern, C. L.; Poeppelmeier, K. R. The Polar [WO<sub>2</sub>F<sub>4</sub>](<sup>2-</sup>) Anion in the Solid State. *Inorg. Chem.* **1999**, *38*, 762.
- (48) Donakowski, M. D.; Gautier, R.; Yeon, J. H.; Moore, D. T.; Nino, J. C.; Halasyamani, P. S.; Poeppelmeier, K. R. The Role of Polar, Lambda (Lambda)-Shaped Building Units in Noncentrosymmetric Inorganic Structures. *J. Am. Chem. Soc.* **2012**, *134*, 7679.
- (49) Gautier, R.; Gautier, R.; Chang, K. B.; Poeppelmeier, K. R. On the Origin of the Differences in Structure Directing Properties of Polar Metal Oxyfluoride MO<sub>x</sub>F<sub>6-x</sub> (<sup>2-</sup>) (x=1, 2) Building Units. *Inorg. Chem.* **2015**, *54*, 1712.
- (50) Marvel, M. R.; Lesage, J.; Baek, J.; Halasyamani, P. S.; Stern, C. L.; Poeppelmeier, K. R. Cation-Anion Interactions and Polar Structures in the Solid State. *J. Am. Chem. Soc.* **2007**, *129*, 13963.



